E11843

# Premixed-gas flame propagation in Hele-Shaw cells*

J. Sharif, M. Abid and P. D. Ronney
Department of Aerospace and Mechanical Engineering
University of Southern California, Los Angeles CA 90089-1453

## Introduction

It is well known that buoyancy and thermal expansion affect the propagation rates and shapes of premixed gas flames. The understanding of such effects is complicated by the large density ratio between the reactants and products, which induces a baroclinic production of vorticity due to misalignment of density and pressure gradients at the front, which in turn leads to a complicated multi-dimensional flame/flow interaction. The Hele-Shaw cell, *i.e.*, the region between closely-spaced flat parallel plates, is probably the simplest system in which multi-dimensional convection is present, consequently, the behavior of fluids in this system has been studied extensively (Homsy, 1987). Probably the most important characteristic of Hele-Shaw flows is that when the Reynolds number based on gap width is sufficiently small, the Navier-Stokes equations averaged over the gap reduce to a linear relation, namely a Laplace equation for pressure (Darcy's law).

In this work, flame propagation in Hele-Shaw cells is studied to obtain a better understanding of buoyancy and thermal expansion effects on premixed flames. This work is also relevant to the study of unburned hydrocarbon emissions produced by internal combustion engines since these emissions are largely a result of the partial burning or complete flame quenching in the narrow, annular gap called the "crevice volume" between the piston and cylinder walls (Heywood, 1988). A better understanding of how flames propagate in these volumes through experiments using Hele-Shaw cells could lead to identification of means to reduce these emissions.

## Theoretical Background

Joulin and Sivashinsky (1994) (hereafter JS) analyzed propagating fronts in Hele-Shaw cells assuming Euler-Darcy flow (where the convection of momentum term is retained, but still averaged across the cell gap). The flame was treated as a interface between burned and unburned gas with constant flame speed averaged across the cell gap. JS described the instability modes due to thermal expansion (the Darrieus-Landau (DL) instability), buoyancy (the Rayleigh-Taylor instability (RT) instability) and the viscosity change across the flame front (the Saffman-Taylor (ST) instability), the last of these being unique to Hele-Shaw cells. All of these are essentially hydrodynamic instabilities that do not depend on flame structure. The instability growth rates ($\sigma$) predicted by JS for typical values of the physical parameters are shown in Fig. 1 for upward, horizontal and downward propagation. Note that only for downward propagation are any wavelengths stabilized ($\sigma < 0$), and even in this case buoyancy is only able to stabilize the longer wavelengths. Thus, according to the JS analysis, for any orientation wrinkles of arbitrarily small wavelength could appear on the front.

One important flame instability mechanism not considered by JS is the diffusive-thermal (DT) mechanism resulting from the unequal rates of diffusion of thermal energy and reactants at the flame front. When the Lewis number (Le) is less than a critical value slightly less than unity, cellular flames occur, which are characterized by $\sigma$ real and having a maximum positive value at a finite wavenumber, whereas for Le greater than the critical value, wrinkling is discouraged ($\mathrm{Re}(\sigma) < 0$ for all $\sigma$). Since this instability is dependent on diffusional effects that occur on the scale of the flame thickness, it has no effect on very long wavelengths and at short wavelengths it is so dominant that diffusion damps out all wrinkling. This prevents arbitrarily small wrinkles (which could otherwise be permitted by the DL, ST and RT mechanisms) from appearing.

To our knowledge, Hele-Shaw cells have not been previously exploited for the experimental study of flame instabilities. The only experimental study of flame propagation in narrow channels known to us is that by Jarosinsky (1983), who studied near-limit flames in narrow plane channels. He did not provide photographs of the fronts nor describe the front shapes in these channels, since his interest was in determining quenching conditions. Consequently, the goal of this study is to examine flame instabilities and propagation rates in Hele-Shaw cells, and to compare these observations to the JS predictions.

*Spring Technical Meeting, joint U. S. Sections, Combustion Institute, Washington, D.C., March 15-17, 1999. Work supported by NASA-Lewis under grants NAG3-1523 and NAG3-2124.

## Apparatus and procedures

The apparatus consisted of two 533 x 737 x 12.7 mm Plexiglas plates and one aluminum plate of the same dimensions, but with a 394 x 597 mm cutout in the middle (Fig. 2). This cutout formed the chamber where the gaseous mixtures were burned. The large cutout dimensions came about from the need to observe unstable wavelengths that are much larger than the cell thickness. The two Plexiglas plates sandwiched the aluminum plate. O-ring seals on both sides of the aluminum plate prevented gas leakage. The gas mixtures were prepared by the partial pressure method. The gases were mixed into a 2 liter mixing chamber, then transferred into the Hele-Shaw apparatus. A spark generator was used to ignite the mixture via two spark electrodes that penetrated through the two Plexiglas plates. To avoid pressure buildup within the cell, a set of relief ports connected through a manifold to a 3/4" ball value was employed. These ports were at the ignition end of the cell, so that the flames propagated toward the closed end of the cell. The ball valve was opened to the ambient atmosphere simultaneously with ignition. Images of the propagating front was recorded by a standard VHS video camera and analyzed using a digital image processing system.

## Results and discussion

For practically all experiments, three distinct stages of propagation behavior were observed, as illustrated in Fig. 3:

- Stage A: thermal expansion. This occurs between the time of ignition and when the flame first reaches the cell side walls. In this stage the fronts are very smooth with few if any wrinkles. The ratio of the observed propagation rate ($S_T$) to the laminar burning velocity ($S_L$) in this stage is nearly constant and comparable to the ratio of reactant to product density, therefore, the front is propagating outward while riding on its own burned gases, as in a spherically expanding flame.
- Stage B: quasi-steady propagation. Almost simultaneously, the flame reaches the cell boundary and small-scale wrinkles (typically 1 cm wavelength) appear on the flame front. Apparently the sudden transition from the nearly radial flow pattern to a more nearly unidirectional flow (toward the end of the cell where the relief ports are located) causes a major change in the instability characteristics. The propagation rate quickly reaches a quasi-steady value that is much lower than the value during Stage A because the front is no longer riding on its thermal expansion.
- Stage C: end-wall effects. The flame nears the end wall of the cell and the large-scale wrinkling is suppressed. The flame speed decreases correspondingly.

Example flame images are shown in Figs. 4a-d. *These images show that wrinkling is observed for all orientations with respect to the gravity vector, even downward.* The small-scale wrinkling is similar for all orientations with respect to the gravity vector, while large-scale wrinkling is very different, which is consistent with the predictions shown in Fig. 1. The dominant large-scale wavelength for upward propagation (Fig. 4b) is the largest one that fits in the apparatus. This is consistent with Fig. 1, which shows that $\sigma$ increases without bound as the wavelength increases. The same is true for horizontal propagation (Fig. 4a), but the growth rate is substantially lower in this case and thus the front is not as curved on the large scale for horizontal as for upward propagation. In fact, for the horizontal case Fig. 1 shows that the ST mechanism adds only a modest increase in growth rate over the DL mechanism alone. For downward propagation (Fig. 4c), only small wavelengths are unstable and thus the front is flat overall on the large scale. Thus, the JS model seems to be consistent with these experimental observations. Comparison of Figs. 4a and 4d show that at lower/higher Le, the flame fronts are rougher/smoother on smaller scales, but even for high Le, wrinkling occurs on larger scales. This is consistent with the predictions of the diffusive-thermal mechanism, which is only effective at small wavelengths.

Figure 5 shows the quasi-steady propagation rates ($S_T$), referenced to $S_L$, observed during Stage B, as a function of the Peclet number. Of course, a Peclet number of greater than about 40 is needed to avoid quenching (Jarosinsky, 1983). Note that for all cases $S_T$ can be significantly greater than $S_L$, with an average value of $S_T/S_L$ of about 2.5 overall, which shows the enhancement of propagation rate due to wrinkling from the instability mechanisms described above. There is only a small effect of Pe on $S_T/S_L$, with a slight decrease in $S_T/S_L$ with increasing Pe for upward propagation, and a slight increase with Pe for downward propagation. This relative lack of Pe dependence is somewhat unexpected since the impact of heat loss scales as $Pe^{-2}$ (Williams, 1985). At lower Pe the heat loss effects are expected to weaken the DL and ST instabilities since heat loss decreases the density and viscosity changes on large scales where

significant cooling can occur. Thus, significantly less wrinkling and lower $S_T/S_L$ might have been expected at lower Pe, but such a trend was not observed. Figure 5 also shows that at a given Pe, for most cases $S_T/S_L$ is highest for upward propagation, lowest for downward propagation, and intermediate for horizontal propagation. This is certainly expected based on the JS predictions shown in Fig. 1, since the growth rates of the instabilities follow this trend. Furthermore, Fig. 5 shows that $S_T/S_L$ is possibly slightly lower overall for higher Le ($C_3H_8$-air mixtures). Again, this would expected since low/high Le encourages/discourages wrinkling and thus promotes more/less rapid flame propagation, though the effect is minor since only the small-scale wrinkling, which contributes relatively little to the overall flame surface area, is affected in this way.

## Conclusions

The behavior of propagating fronts were studied in Hele-Shaw cells. Fronts with a variety of laminar propagation rates ($S_L$) and Lewis numbers were examined. Wrinkles of varying sizes were observed. Significantly, wrinkling was observed even for downward propagating (buoyantly stable) flames have high Le (diffusive-thermally stable). The Joulin-Sivashinsky (JS) model describes most of the experimental observations. The burning rates of these flames are quite different from their laminar, unwrinkled values. Flame development proceeded in three stages, the first characterized by radially outward propagation dominated by thermal expansion, the second by unidirectional quasi-steady propagation and the last by end-wall effects. Values of $S_T/S_L$ in the quasi-steady stage were higher for upward vs. downward propagation, but only weakly dependent on Lewis and Peclet numbers. The first of these effects is consistent with the JS model, whereas the last is contrary to the JS predictions concerning the effects of heat losses.

These results indicate that the behavior of flame propagation in narrow channels such as crevice volumes in premixed-charge internal combustion engines may be quite different from that inferred from simple laminar flame experiments. This behavior is particularly noteworthy because flame quenching in crevice volumes is an important source of unburned hydrocarbon emissions in these engines.

## References


Heywood, J. B. (1988). *"Internal Combustion Engine Fundamentals,"* McGraw-Hill, New York.

Homsy, G. M. (1987). "Viscous Fingering in Porous Media," *Ann. Rev. Fluid Mech.*, Vol. 19, p. 271.

Jarosinsky, J. (1983). "Flame Quenching by a Cold Wall," *Combust Flame.* Vol. 50, p.167.

Joulin , G. and Sivashinsky, G. I. (1994). "Influence of Momentum and Heat Losses on the Large-Scale Stability of Quasi-2D Premixed Flames," *Combust. Sci. Tech.*, Vol. 98, p.11.

Sivashinsky, G. I. (1977). "Diffusional Thermal Theory of Cellular Flames," *Combust. Sci. Tech.*, Vol. 15, p.137.

Williams, F. A. (1985). *"Combustion Theory,"* Benjamin-Cummings, Menlo Park, CA.


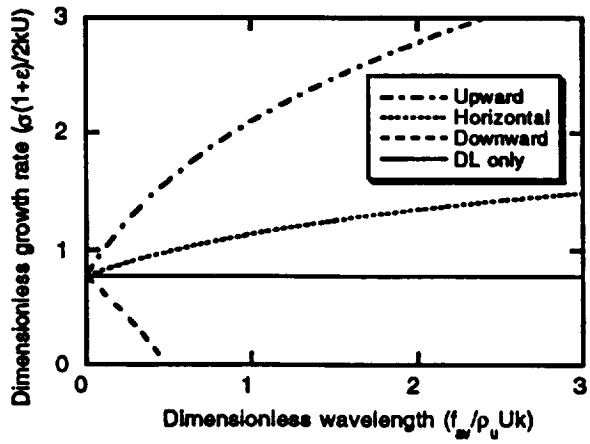


Figure 1. Dimensionless growth rate vs. dimensionless wavelength according to the Joulin-Sivashinsky analysis, for conditions representative of 7.5% $CH_4$ in air with 12.7 mm gap width.

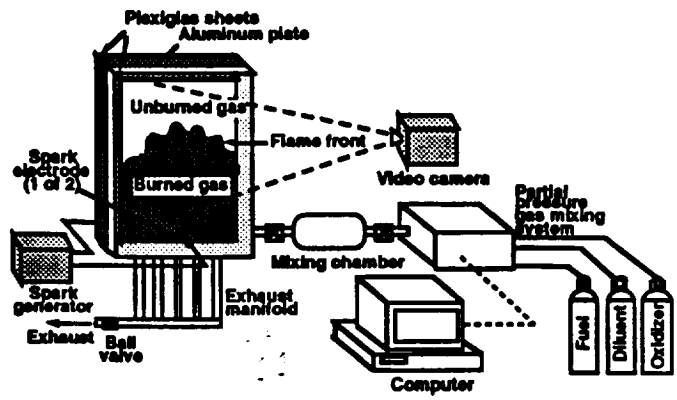


Figure 2. Apparatus for gaseous combustion experiments in Hele-Shaw cells.

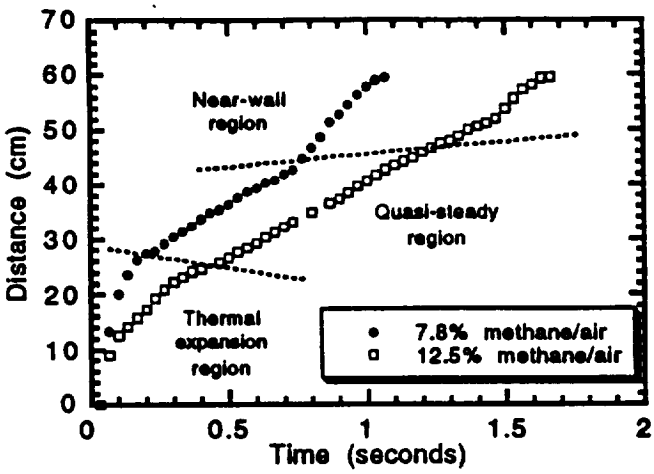


Figure 3. Examples of flame propagation distance vs. time for downward propagating $CH_4$-air flames.

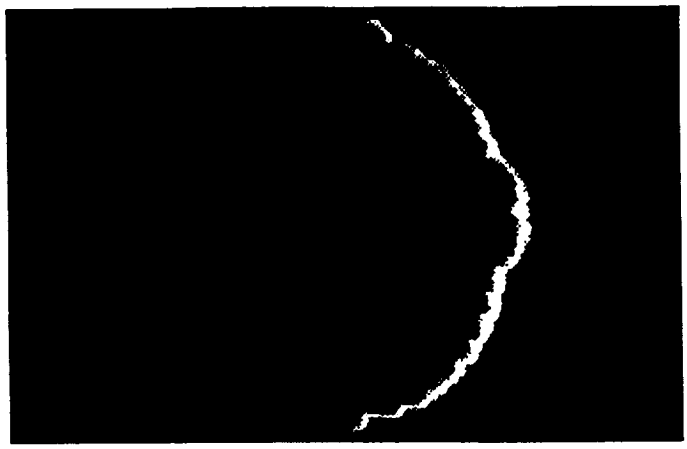

Figure 4. Images of flames in Hele-Shaw cells: (a) 7.2% $CH_4$ in air, horizontal propagation, 0.27 s after ignition. Flame propagates from left to right. Field of view is 394 mm x 597 mm.

Figure 4. Images of flames in Hele-Shaw cells: (b) 7.1% $CH_4$ in air, upward propagation, 0.30 s after ignition. Flame propagates from left to right. Field of view is 394 mm x 597 mm.

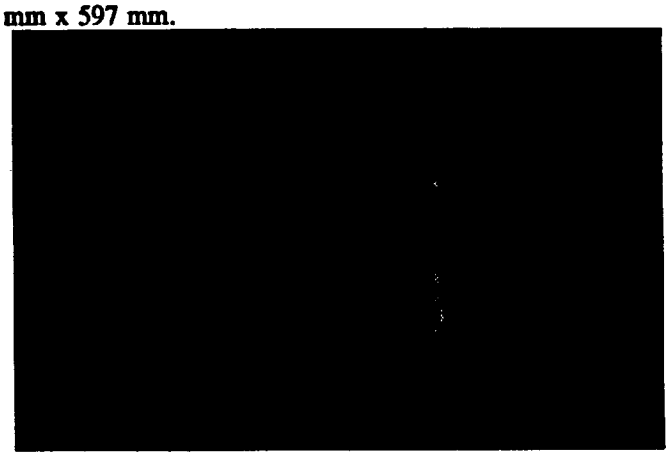

Figure 4. Images of flames in Hele-Shaw cells: (c) 7.1% $CH_4$ in air, downward propagation, 0.83 s after ignition. Flame propagates from left to right. Field of view is 394 mm x 597 mm.

Figure 4. Images of flames in Hele-Shaw cells: (d) 7.1% $C_3H_8$ in air, horizontal propagation, 0.30 s after ignition. Flame propagates from left to right. Field of view is 394 mm x 597 mm.

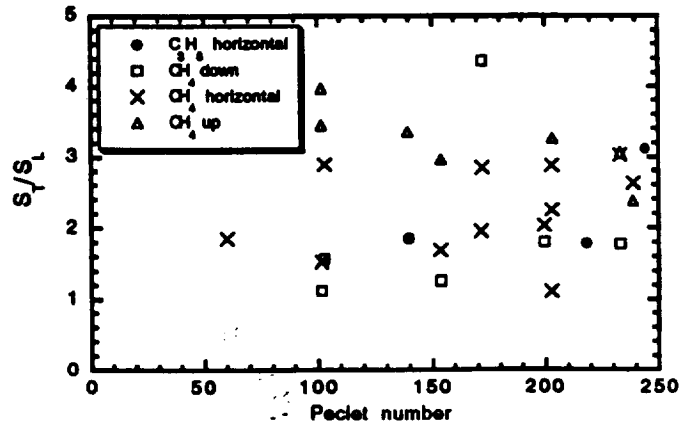


Figure 5. Correlation of wrinkled front speed ($U_T$) with Peclet number for gaseous flames in Hele-Shaw cells.